

Assimilative Real-time Models of HF Absorption at High Latitudes

Neil C. Rogers¹, Farideh Honary¹, Jonathan Hallam², Alan J. Stocker²,
E. Mike Warrington², Dave R. Siddle², Donald W. Danskin³ and Bryn Jones⁴

¹ Dept. of Physics, Univ. of Lancaster, UK; ² Dept. of Engineering, Univ. of Leicester, UK;
³ Natural Resources, Canada; ⁴ SolarMetrics ltd, UK

ABSTRACT

Improved real-time HF communications frequency management is required for aircraft on trans-polar routes. Polar cap absorption (PCA) models have therefore been adapted to assimilate real-time measurements of zenithal cosmic radio noise absorption (~ 30 MHz) from a large network of online riometers in Canada and Finland. Two types of PCA model have been developed and improvements to model accuracy following optimisation are quantified. Real-time optimisation is performed by age-weighting riometer measurements in a non-linear regression. This reduces root-mean-square errors (RMSE) from 2-3 dB to less than 1 dB and mean errors to within ± 0.2 dB over a wide latitude range. This paper extends previous work by further optimising the models' dependences on solar-zenith angle to account for differences in the ionospheric response at sunrise and sunset (the Twilight Anomaly). Two models of the rigidity cutoff latitudes are compared and one is optimised in real time by regression to riometer measurements. Whilst measurements from the NASA POES satellites may provide a direct measurement of the rigidity cut-off, it is observed that proton flux measurements from POES often need correcting for relativistic electron contamination for several hours at the start of a PCA event. An optimised real-time absorption model will be integrated into HF ray-tracing propagation predictions relating to measurements of HF signal strengths on a network of HF transmitters and receivers in the high northern latitudes.

1. INTRODUCTION

The high-latitude ionosphere presents a challenging environment in which to forecast HF radiowave propagation. The presence of horizontal electron density gradients associated with the mid-latitude trough and F-region polar patches produce large azimuthal deviations from the great-circle path [Warrington *et al.*, 2012, 1997; Rogers *et al.*, 1997], sporadic E layers can alter the mode of propagation [Stocker and Warrington, 2011; Ritchie and Honary, 2009] affecting the signal multipath and Doppler spread [Stocker *et al.* 2013], and ionisation enhancements from precipitating energetic particles or solar-flare x-ray flux enhancements increase absorption of the HF radio waves [Rogers and Honary, 2015 and references therein].

A new service is being developed to accurately monitor and predict HF link availability, designed principally for air traffic controllers and airlines that operate services on polar routes. Measurement of signal characteristics and a real-time ray-path model of propagation are being provided by the University of Leicester, UK in collaboration with Natural Resources Canada [Warrington *et al.*, 2015]. These will incorporate real-time models of HF absorption resulting from ionisation enhancements in the ionosphere, which are the focus of this paper.

The work has initially focused on the most intense HF absorption events – Polar Cap Absorption [Bailey, 1964] (PCA) – which result from energetic proton precipitation into the polar D-region ionosphere. At lower latitudes the geomagnetic field shields all but the highest energy protons (those below a threshold ‘rigidity’ (momentum per unit charge)). PCA events are associated with Solar Proton Events (SPE), where the flux of > 10 MeV solar protons, $J(> 10 \text{ MeV})$, exceeds 10 proton flux units ($1 \text{ pfu} = 1 \text{ cm}^{-2} \text{ sr}^{-1} \text{ s}^{-1}$). Up to 20 SPEs occur per year near solar maximum (see <http://umbra.nascom.nasa.gov/SEP/>) and the largest of these events may persist for several days.

2. MEASUREMENTS

The measurement of HF radiowave absorption is most effectively determined using riometers, which measure the intensity of cosmic radio noise on a zenithal beam in a quiet radio band at approximately 30 MHz. The ionospheric absorption (in dB) is determined by comparison with a “quiet day curve” (QDC), which is the average variation of cosmic noise over the sidereal day, determined from recent recordings in which no significant absorption events were apparent. The measurements presented in this paper are from up to 13 riometers in the Canadian Space Agency / University of Calgary NORSTAR array [Rostoker *et al.*, 1995], complemented by the IRIS riometer in Kilpisjärvi, Finland, operated by Lancaster University and the Sodankylä Geophysical Observatory (SGO). These measurements were filtered to remove periods of extraneous noise (when measured cosmic noise exceeded the QDC minus a margin of 0.1 dB), calibration signals, periods up to 6 hours following Storm Sudden Commencements / Sudden Impulses, and very low intensity signals (< 0.2 V raw signal power) which were potentially subject to inaccurate calibration. The geostationary NASA GOES satellites provided measurements of the omnidirectional energetic solar proton flux at multiple energy thresholds and the X-ray flux in the 0.1-0.8 nm band. The proton flux spectrum is also measured from the polar-orbiting NASA POES satellites as described in Section 6.

3. POLAR CAP ABSORPTION (PCA) MODELS

Two types of PCA model have been implemented in a form that permits the optimisation of their key parameters:

- i. **Type 1 models** relate absorption to the square-root of near-Earth proton flux integrated above an energy threshold, $J(> E_t)$. An example is the real-time online D-Region Absorption Prediction service (DRAP) [Sauer and Wilkinson, 2008] (S&W) provided by the US National Oceanic Atmospheric Administration (NOAA) Space Weather Prediction Center (SWPC).
- ii. **Type 2 models** use model altitude profiles of the constituent neutral gas densities and temperatures, which, together with measurements of the energy spectrum of precipitating protons, determine a profile of the ionisation rate in the D-region. A model profile of the effective recombination coefficient $\alpha_{eff}(z)$ is then used to determine the steady-state electron density profile $N_e(z)$ which defines the specific absorption (dB/km) as a function of altitude, z . The Type 2 model in this paper is based on [Patterson *et al.*, 2001] but with neutral atmospheric profiles determined from the NRLMSISE-00 model [Picone *et al.*, 2002].

For both model types, a component of absorption, A_x , due to solar X-ray ionisation is added for the sunlit ionosphere using the empirical model [Schumer, 2009 (p.49)] used in DRAP. Energetic particles (principally electrons) precipitating from the magnetospheric radiation belts also contribute to HF absorption in the auroral zones but this component has been neglected in this paper on the assumption that it is a secondary effect during PCA events.

3.1. PROTON RIGIDITY CUT-OFFS

The differential proton flux spectrum $J(E)$ (pfu MeV^{-1}) is cut off at energies below a threshold, E_c , which is modelled as a function of geomagnetic latitude, geomagnetic activity indices (e.g. K_p , D_{st}) and, in some cases, the magnetic local time (MLT). DRAP utilises the rigidity cutoff model of [Smart *et al.*, 1999] derived from SAMPEX satellite measurements and particle ray-tracing through a model magnetosphere. The performance of DRAP has been compared with a similar model in which the cutoff model of [Dmitriev *et al.*, 2010] is substituted. The Dmitriev rigidity cutoffs were determined from proton fluxes measured on the POES satellites. Whilst other cutoff models have been developed from POES measurements (see [Nesse Tyssøy and Stadsnes, 2015] and references therein), until recently the Dmitriev model was unique in incorporating the fluxes of protons at the lower energies (< 16 MeV) which are important for HF absorption modelling. Lower energy proton cutoff boundaries also exhibit a stronger MLT asymmetry. Figure 1 compares the 10 MeV proton cutoff predicted from the Smart and Dmitriev models (dashed lines) with measured CNA on a line of seven NORSTAR riometers lying close to the 94°W geographic meridian ($\pm 2^\circ$) from Taloyoak

(69.5°N,93.6°W) in the north to Pinawa (50.2°N,96.0°W) in the south. This comparison demonstrates that the Smart model cutoff lies approximately 2-3° poleward of that observed from riometer measurements. This is broadly in agreement with the findings of *Leske et al.* [2001] (based on SAMPEX proton flux observations) and *Neal et al.* [2013] (based on POES measurements).

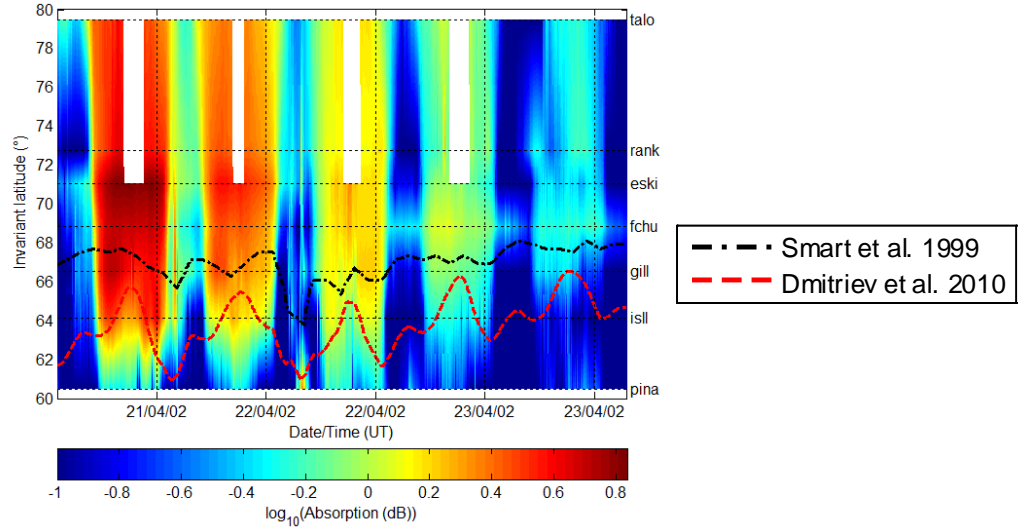


Figure 1. Two models of the cutoff latitude of 10 MeV protons (dashed lines) for the SPE of April 2002. Colours represent 30 MHz Cosmic Noise Absorption measured on seven riometers near the 94°W meridian, interpolated linearly in invariant latitude.

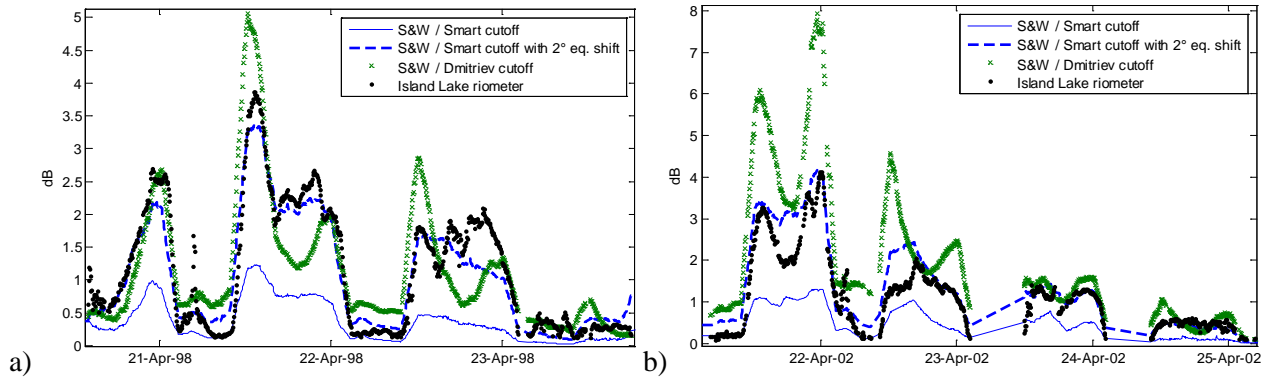


Figure 2. 30 MHz absorption at the Island Lake riometer during SPEs in a) April 1998 and b) April 2002 compared with predictions of S&W model (which uses the Smart cutoff model), S&W with a 2° equatorward shift of the Smart cutoff, and S&W with CL defined by (*Dmitriev et al.*, 2010).

Figure 2 presents an example of absorption measurements from the Island Lake (isll) riometer (53.9°N, 265.3°E) (black ‘◇’s) during the SPE of April 1998, compared with the DRAP (S&W) predictions (blue solid line). Shifting the Smart cutoff latitude equatorward by $\Delta\lambda=2^\circ$ in invariant latitude (blue dashed line) provides a better fit to the measurements. Replacing the Smart model with the Dmitriev cutoff model also improves the fit (green ‘×’s) during the daytime, but the predicted dip in absorption near local noon (17:41 UT) is not always observed in the measurements. Further analysis of multiple riometer measurements over all solar proton events 1996-2010 has shown that applying an equatorward shift in invariant latitude, $\Delta\lambda$, of 2-3° to the Smart model cutoff latitudes minimised the errors associated the S&W model [*Rogers and Honary*, 2015].

4. OPTIMISATION OF PCA MODEL PARAMETERS

The Type 1 PCA model may be expressed in a generalised form in which the 30 MHz absorption estimate is

$$\hat{A} = A_n(1 - Z_a) + A_d Z_a + S \sin\left(2\pi \frac{MLT}{24}\right) + C \cos\left(2\pi \frac{MLT}{24}\right) + D \sin\left(\frac{\pi}{2} \frac{\delta}{23.44^\circ}\right) \quad (\text{dB}) \quad (1)$$

The first two terms of (1) describe the original S&W model in which

$$A_n = \mathbf{m}_n J^n (> \max(\mathbf{E}_{tn}, E_c)) \quad (\text{dB}) \quad (2)$$

$$A_d = \mathbf{m}_d J^n (> \max(\mathbf{E}_{td}, E_c)) \quad (\text{dB}) \quad (3)$$

are the night and daytime absorption values, the exponent n is 0.5 (a square root relation) and other fixed parameters are $\mathbf{m}_n = 0.020$, $\mathbf{m}_d = 0.115$, $\mathbf{E}_{tn} = 2.2$ MeV, $\mathbf{E}_{td} = 5.2$ MeV, where the subscripts n and d represent night and day values, respectively. The absorption prediction in the region of the solar terminator adopted by the S&W model is a linear interpolation between absorption predictions in the fully-developed day and night ionospheres, which may be expressed as a ‘daytime weighting factor’:

$$Z_d = \begin{cases} 1, & \chi \leq \chi_l \quad (\text{day}) \\ (\chi_u - \chi) / (\chi_u - \chi_l), & \chi_l < \chi < \chi_u \quad (\text{twilight}) \\ 0, & \chi \geq \chi_u \quad (\text{night}) \end{cases} \quad (4)$$

where χ is the solar-zenith angle. In the S&W model the transition region is bounded by $\chi_l = 80^\circ$ and $\chi_u = 100^\circ$. The last three terms in (1) are optional, but allow the model to be optimised such that it incorporates residual variations in absorption (relative to quiet pre-SPE conditions) as a function of MLT (terms including S and C), and seasonal variations parameterised by the mean solar declination, δ , with magnitude D .

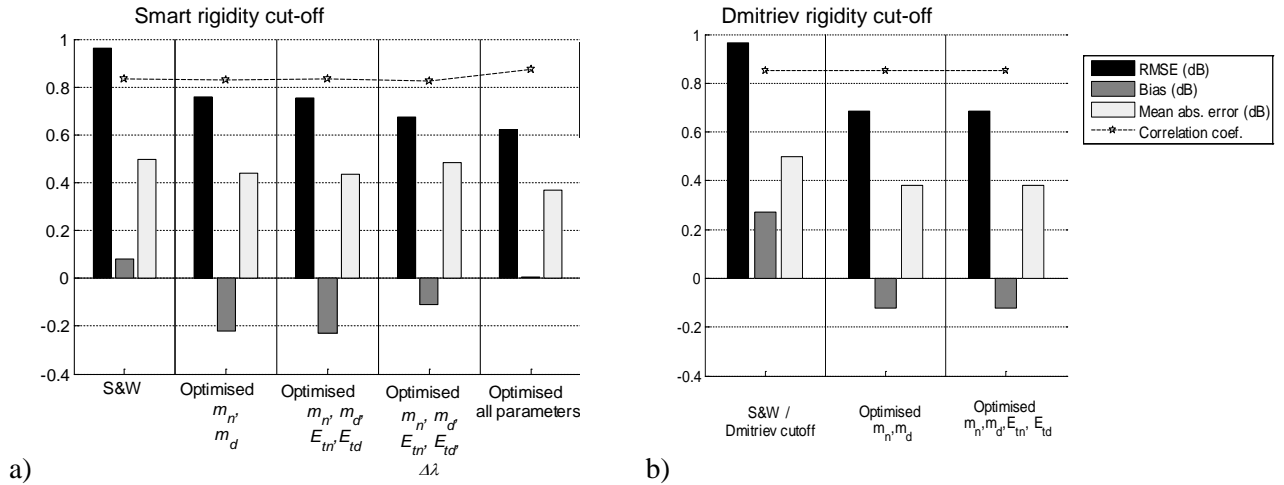


Figure 3: Error statistics for 94 SPEs and 14 riometers following optimisation of selected parameters (equations (1)-(4)). a) Original Smart cutoff model, b) Dmitriev cutoff model.

The parameters in bold typeface in (1)-(4) have been optimised by non-linear regression to riometer measurements from all 94 SPEs in the period 1996-2010. Optimisations improve the root-mean-squared error (RMSE), bias (the mean error (model - measurement)), mean absolute error and the Pearson correlation coefficient as presented in Figure 3a (using the Smart rigidity cut-off model) and Figure 3b (substituting the Dmitriev cut-off). The first set of bars represents errors associated with the un-optimised S&W model, whilst the other sets represent optimisation of selected parameters from the set $\{\mathbf{m}_n, \mathbf{m}_d, E_{tn}, E_{td}, \Delta\lambda, n, \chi_l, \chi_u, S, C, \text{ and } D\}$ labelled on the abscissae. Substituting the Dmitriev cutoff model yields improvements similar to the case in which the cutoff latitude offset $\Delta\lambda$ is optimised in the Smart model, although the greatest improvements are obtained by optimising all parameters, reducing RMSE by 36% from 1 dB to 0.6 dB and effectively eliminating the model bias.

The fixed parameters of the daytime weighting factor, Z_d (equation (4)) in the S&W model are identical for sunrise and sunset. There is, however, a well-documented difference in behaviours for sunrise and sunset referred to as the ‘‘Twilight anomaly’’ [Ranta *et al.*, 1995; Hargreaves *et al.*, 1993]. Figure 4 presents the quantity $m_{10} = A/\sqrt{J(> 10 \text{ MeV})}$ measured at the Fort Churchill riometer (58.8°N, 265.9°E) separately for a) sunrise and b) sunset periods for the multi-day SPE of April 2002 – a quantity analogous to the m_n and m_d parameters in (2) and (3). These plots indicate that the tri-linear weighting function $Z_d(\chi)$ in the S&W

model is an appropriate model form, but that the chosen limiting values of $\chi = 80^\circ$ and 100° should be modified to approximately 70° and 98° for sunrise, and 88° and 98° at sunset. Figure 4 also illustrates the considerable day-to-day variation in the value of the day and night values of m_{10} , indicating a need to update the optimisation of the values of m_n and m_d on at least a daily basis. It is possible to optimise the χ thresholds in (4) independently for sunrise and sunset. Figure 5 presents error statistics based on SPE measurements for all 14 riometers, based on the original S&W model (left), a version with optimising parameters $\{m_n, m_d, E_{tn}, E_{td}, \Delta\lambda\}$ (centre) and a version with optimised $\{m_n, m_d, E_{tn}, E_{td}, \Delta\lambda, \chi_l(sr), \chi_l(ss), \chi_u(sr), \chi_u(ss)\}$ (right), where sr denotes sunrise, and ss denotes sunset. The resulting optimum zenith angle boundaries obtained are $\chi_l(sr) = 69.24^\circ$, $\chi_l(ss) = 81.01^\circ$, $\chi_u(sr) = 100.15^\circ$, $\chi_u(ss) = 101.49^\circ$. Applying these limits improves RMSE, bias and mean absolute errors although the improvements are marginal since relatively few measurements are made near these boundaries.

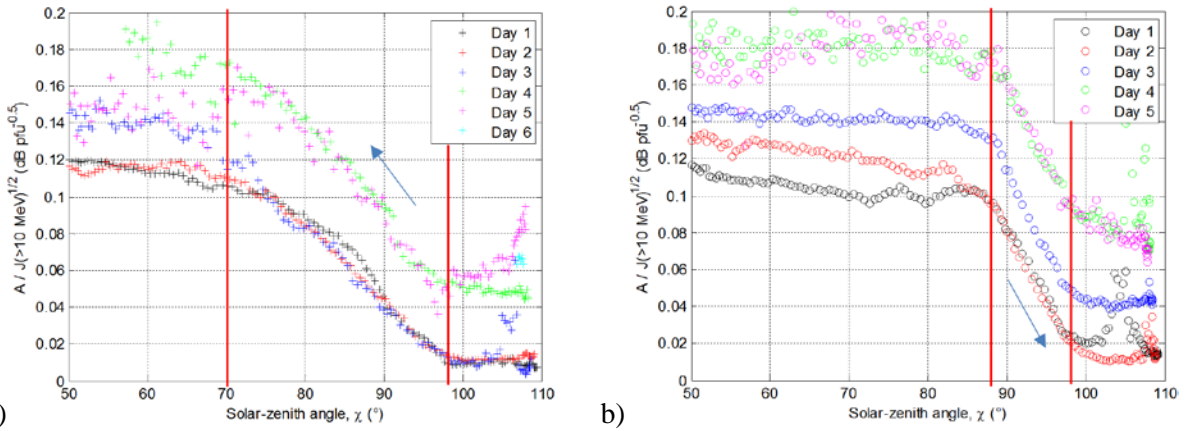


Figure 4. Ratio of absorption (dB) at the Fort Churchill riometer to the square root of > 10 MeV proton flux for the SPE commencing 21 April 2002 as a function of solar-zenith angle. a) sunrise, b) sunset. The arrows indicate the change in χ with time.

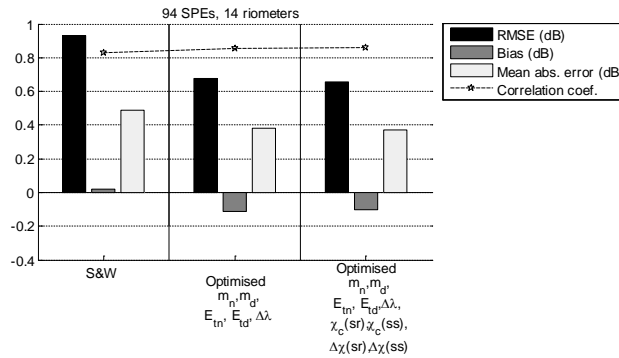


Figure 5. PCA model errors following optimisation of selected parameters of the S&W model (equations (1)-(4)) (with Smart model rigidity cutoff).

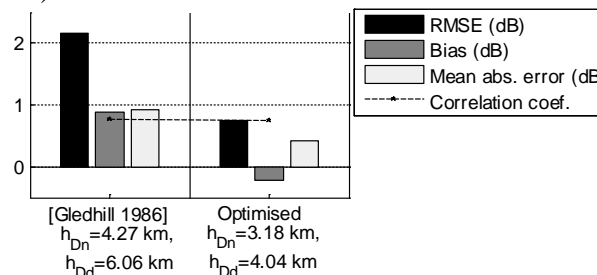


Figure 6. Type 2 PCA model errors before and after optimising D-region $\alpha_{eff}(z)$ scale heights for all 94 SPEs 1996-2010.

Optimisation of the Type 2 PCA model was performed by varying the night and daytime scale heights, h_{Dn} and h_{Dd} , of the effective recombination coefficient profile $\alpha_{eff}(z)$ in the D-region. Optimisations based on

regression to measurements for all 94 SPEs and all 14 riometers led to a 66% reduction in the RMS error and substantial improvement in the model bias and mean absolute errors as shown in Figure 6.

5. REAL-TIME OPTIMISATION

The PCA model parameters have been optimised by a weighted regression in which the weights w_i diminish with the age of each measurement, Δt_i , at a rate determined by a characteristic time, τ . Thus $w_i = 1 + N \exp(-\Delta t_i/\tau)$. With this weighting, if there are no recent measurements, the model reverts to the optimum parameters determined for the complete data set of N measurements. Figure 7 presents an example of the real-time optimised absorption predictions (red '+') during the July 2000 SPE, alongside measurements at the Rankin Inlet riometer (62.8°N, 267.9°E) (black \diamond) compared with the un-optimised S&W (DRAP) predictions (blue '+'). Optimisations utilised all available riometer measurements, age-weighted using $\tau=6$ h and the values of the optimised parameters are shown in Figure 8. Real-time optimisation provides an improved fit to the measurements although some optimised model parameters can be highly variable and could benefit from greater smoothing.

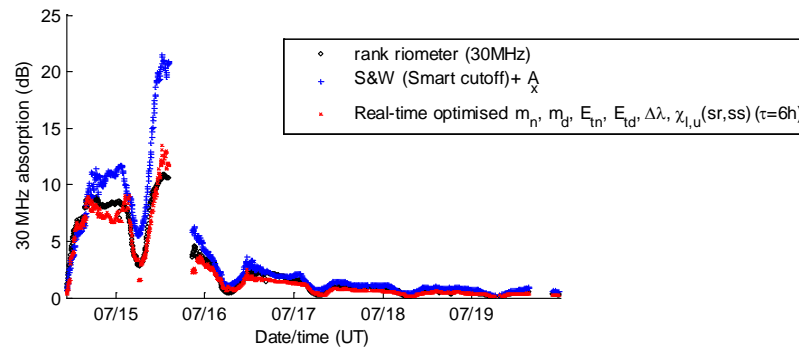


Figure 7. S&W (DRAP) predictions of absorption during the July 2000 SPE (blue '+') at the Rankin Inlet riometer (black \diamond) and real-time-optimised m_n , m_d , E_{tn} , $\Delta \lambda$ (using all riometers) $\tau = 6$ h.

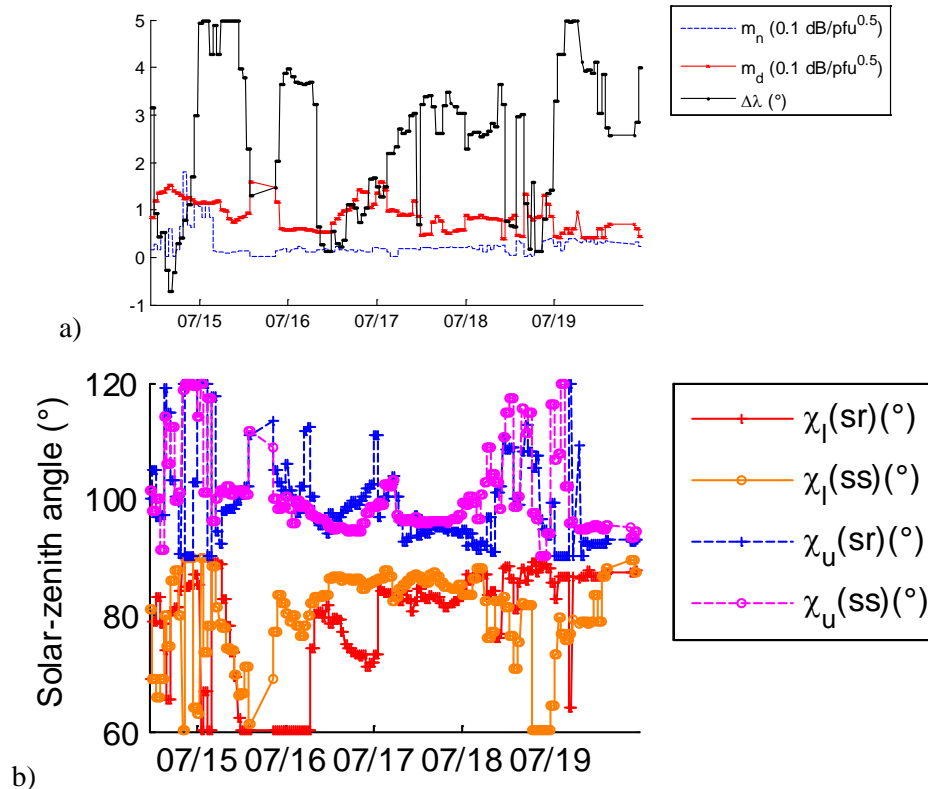


Figure 8. Real-time optimised parameters determined for the times shown in Figure 7. a) m_n , m_d and $\Delta \lambda$, b) $\chi_l(sr)$, $\chi_l(ss)$, $\chi_u(sr)$ and $\chi_u(ss)$.

A statistical analysis of error metrics has been performed for 13 large, multi-day SPEs for a simple practicable scenario in which a single polar cap riometer was used to optimise Type 1 and Type 2 models for a meridional chain of riometers. The results (detailed in [Rogers and Honary, 2015]) demonstrate improvements in RMSE from 2-3 dB to less than 1 dB and mean errors to within ± 0.2 dB over a wide latitude range.

6. ASSIMILATION OF POES PROTON FLUX MEASUREMENTS

The POES satellites measure energetic proton fluxes from sun-synchronous orbits between 800 and 900 km altitude. These can provide direct near-real-time observations of the rigidity cut-off boundary during an SPE (e.g. applying the algorithm of Neal *et al.* [2013], based on [Leske *et al.*, 2001]). The proton flux spectrum measured by the POES satellite MEPED sensors may also be directly converted to CNA absorption measurements. This is demonstrated in Figure 9, which compares absorption measurements determined from the DRAP algorithm for GOES measurements (blue '+') with those determined from POES measurements (red 'o') for the SPE commencing 14:10 UT on 15 April 2001.

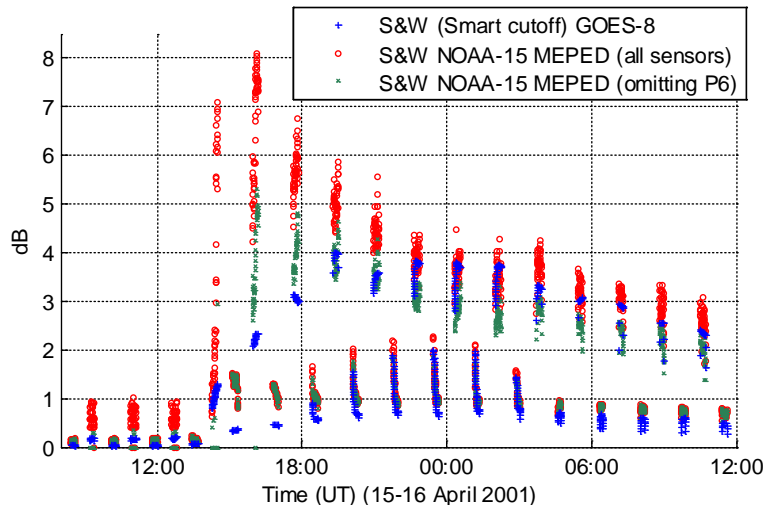


Figure 9. 30 MHz absorption predicted by the S&W model at the POES satellite (foot-of-field-line) at high latitudes ($L > 6$) for the initial phase of an SPE commencing 14:10 UT on 15 April 2001. Omnidirectional proton flux is determined at GOES (blue '+'), POES using all MEPED sensors (with zenithal 0° telescopes P1 to P6) (red 'o') and POES omitting the P6 (> 6.9 MeV) telescope (green 'x').

The estimates, given at the satellite location (traced to the foot of the magnetic field line) at high latitudes only ($L > 6$), utilise all 9 proton energy channels assume a pitch angle loss-cone half-angle of 30° for the high-energy (> 16 MeV) protons detected by the MEPED omnidirectional sensors, and the conversion of count rates to equivalent omnidirectional flux following the procedure in [Evans and Greer, 2006]. There is a close agreement between GOES and POES-derived absorption estimates only after an initial 6-hour period after SPE commencement in which POES-estimates are significantly higher. This is likely due to contamination of the P6 (> 6900 keV sensor) by relativistic (> 700 keV) electrons, as reported by Rodger *et al.* [2010] (citing [Millan *et al.*, 2008]). Omitting this sensor from the model (and interpolating energy channels) produces a closer match to the GOES-DRAP estimates as shown by the green 'o' in Figure 9.

7. SUMMARY AND CONCLUSIONS

A range of techniques have been developed to optimise the parameters of two types of Polar Cap Absorption models. This can be performed in real-time using an aged-weighted non-linear regression to riometer measurements from multiple locations in Canada and Finland. Measurements may be assimilated from multiple riometers in although even a single polar-cap riometer could improve model performance over a wide latitude range (see [Rogers and Honary, 2015]). This study demonstrates the potential to further optimise the DRAP model [Sauer and Wilkinson, 2008] by varying its solar-zenith angle boundaries independently for sunrise and sunset. It is also demonstrated that assimilation of POES (sun-synchronous orbiting satellite) proton measurements may be beneficial, although during the first six hours of a solar proton

event the P6 (> 6.9 MeV) channel is often contaminated by relativistic electrons and should be omitted from absorption calculations. Further model developments will focus on the incorporation of auroral zone absorption due to electron precipitation and the incorporation of absorption maps into real-time HF propagation models.

ACKNOWLEDGEMENTS

This work was supported by the UK Engineering and Physical Sciences Research Council, grant EP/K007971/1. Operational support for the CANOPUS / NORSTAR instrument array was provided by the Canadian Space Agency. We acknowledge the efforts of Don Wallis who was principally responsible for the scientific operation of the CANOPUS riometer array and the NORSTAR team for providing the riometer data used in this study. We also acknowledge the US National Geophysical Data Centre for providing GOES and POES satellite data.

REFERENCES

- Bailey, D. K. (1964) *Planet. Space Sci.* 12, 495-541.
- Dmitriev, A. V., P. T. Jayachandran and L.-C. Tasi. (2010) *J. Geophys. Res.* 115, A12244.
- Evans, D. S. and M. S. Greer, (2006) *Polar Orbiting Environmental Satellite Space Environment Monitor – 2 Instrument Descriptions and Archive Data Documentation Appendix F Rev. 1.*
- Hargreaves, J. K., A.V. Shirochikov, and A. D. Farmer. (1993) *J. Atmos. Terr. Phys.*, 55 (6), 857–862.
- Leske, R. A., R. A. Mewaldt, E. C. Stone, and T. T. von Rosenvinge (2001), *J. Geophys. Res.*, 106 (A12), 30,011–30,022.
- Millan, R. M., K. Yando, and J. C. Green (2008) *Eos Trans. AGU*, 89(53), Fall Meet. Suppl., Abstract U13A-0043.
- Neal, J. J., C. J. Rodger, and J. C. Green.(2013) *Space Weather*, 11, 420–433.
- Nesse Tyssøy, H., and J. Stadsnes (2015), *J. Geophys. Res. Space Physics*, 120, 553–563.
- Patterson, J. D., T. P. Armstrong, C. M. Laird, D. L. Detrick and A. T. Weatherwax (2001) *J. Geophys. Res.*, 106 (A1), 109-163.
- Picone, J.M., A. E. Hedin, D. P. Drob and A. C. Aikin. (2002) *J. Geophys. Res.*, 107 (A12), SIA 15-1 to 15-16.
- Ranta, H., H. Yamagishi, and P. Stauning. (1995). *Ann. Geophys.*, 13, 262–276, 1995.
- Ritchie, S. E., and F. Honary (2009) *J. Atmos. Sol. Terr. Phys.*, 71(12), 1353–1364.
- Rodger, C. J., M. A. Clilverd, J. C. Green, and M. M. Lam (2010), *J. Geophys. Res.*, 115, A04202.
- Rogers, N. C. and F. Honary (2015) *J. Space Weather Space Clim.*, 5, A8. DOI:10.1051/swsc/2015009.
- Rogers, N. C., E. M. Warrington, and T. B. Jones (1997), *IEE Proc. Microwaves Antennas Propag.*, 14(2), 91–96.
- Rostoker, G., J. C. Samson, F. Creutzberg, T. J. Hughes, D. R. McDiarmid, A. G. McNamara, A. Vallance Jones, D. D. Wallis and L. L. Cogger (1995) *Space Science Reviews*, 71, 743-760.
- Sauer, H. H., and D. C. Wilkinson. (2008) *Space Weather*, 6, S12002.
- Schumer, E. A. (2009) Ph.D. dissertation, AFIT/DS/ENP/09-J01, United States Air Force, Wright-Patterson Air Force Base, Ohio, USA.
- Smart, D. F., M. A. Shea, E.O. Fluckiger, A. J. Tylka, and P.R. Boberg (1999) *Proc. Int. Cosmic Ray Conf.*, 7, 337-340.
- Stocker, A. J., and E. M. Warrington (2011) *Radio Sci.*, 46, RS2002.
- Stocker, A. J., E. M. Warrington, and D. R. Siddle (2013) *Radio Sci.*, 48, 638–645.
- Warrington, E. M., N. C. Rogers, and T. B. Jones (1997), *IEE Proc. Microwaves Antennas Propag.*, 144 (4), 241–249.
- Warrington, E. M., N. Y. Zaalov, J. S. Naylor, and A. J. Stocker (2012) *Radio Sci.*, 47, RS0L13.
- Warrington, E. M., A. J. Stocker, D. R. Siddle, J. Hallam, N. Y. Zaalov, F. Honary, N. C. Rogers, D. H. Boteler, and D. W. Danskin (2015) *Proc. 14th International Ionospheric Effects Symposium*, Alexandria, VA, USA, 12-14 May 2015.